Long Short-Term Memory-Networks for Accurate State of Charge Estimation of Li-ion Batteries

Ephrem Chemali, *Student Member, IEEE*, Phillip J Kollmeyer, *Member, IEEE*, Matthias Preindl, *Member, IEEE*, Ryan Ahmed, *Member, IEEE*, and Ali Emadi, *Fellow, IEEE*

***Abstract*—State of Charge (SOC) estimation is critical to the safe and reliable operation of Li-ion battery packs, which nowadays are becoming increasingly used in Electric Vehicles (EV), Hybrid Electric Vehicles, Unmanned Aerial Vehicles (UAV) and smart grid systems. We introduce a new method to perform accurate State of Charge (SOC) estimation for Li-ion batteries using a Recurrent Neural Network (RNN) with Long Short-Term Memory (LSTM). We showcase the LSTM-RNN's ability to encode dependencies in time and accurately estimate SOC without using any battery models, filters or inference systems like Kalman Filters. In addition, this machine learning technique, like all others, is capable of generalizing the abstractions it learns during training to other datasets taken under different conditions. Therefore, we exploit this feature by training a LSTM-RNN model over datasets recorded at various ambient temperatures leading to a single network which can properly estimate SOC at different ambient temperature conditions. The LSTM-RNN achieves a low Mean Absolute Error (MAE) of 0.573% at a fixed ambient temperature and a MAE of 1.606% on a dataset with ambient temperature increasing from 10°C to 25°C.**

***Index Terms*—Battery Management Systems (BMS), Long Short-Term Memory, Li-ion batteries, Machine Learning, Neural Networks, Recurrent Neural Networks, State of Charge Estimation**

I. Introduction

ACCORDING to the World Health Organization (WHO), 6.5 million people die each year as a result of air pollution. In 2015, the transportation sector accounted for 50% of nitrogen oxide air pollutants, which translates into 53 million tonnes of airborne nitrogen oxide emissions worldwide. About half of the total health-related economic cost due to outdoor air pollution can be attributed to the road transport sector. This was estimated to be $865 billion in 2010 [1]. As a result, some European countries, like Norway, are considering plans to ban petrol and diesel powered vehicles by 2025. This coupled with the significantly higher efficiencies brought about by electrified vehicles is enticing a greater dependency on batteries. Specifically, Li-ion batteries are widely used for this type of application due to their high specific energy [2], [3]. Besides, applications for electrified vehicles, the UAV and smart grid markets are growing and are heavily dependent on Li-ion battery technology.

State of Charge (SOC) estimation is critical to ensure reliable operation of the electric drive since this quantity directly gauges a vehicle's remaining driving range and is necessary for the battery balancing system [3]–[5]. SOC estimation is a cumbersome task since the battery undergoes erratic dynamics during repeated acceleration and deceleration of electrified vehicles. There exists no direct way to measure SOC, therefore it is critical to accurately estimate state of charge [4], [6].

SOC is defined as the remaining charge within the battery pack and is given by the residual capacity of the battery divided by its nominal capacity [3]. In general, the estimation of SOC is a nonlinear function that varies with temperature and discharge/charge currents [7], [8]. Traditionally, two SOC estimation techniques have been used; *open circuit voltage* based techniques and *coulomb counting* [6], [9]. These are commonly known to have their limitations and have been generally displaced by more sophisticated methods. Typically, these methods use an (adaptive) cell model, voltage, and current measurements to issue an estimate, e.g. Luenberger observer [6], [10], adaptive observer [6], [11], sliding mode observer [6], [12], [13], and Kalman Filters [14], [15]. These strategies tend to be computationally intensive and typically require additional parameters or different models to perform SOC estimation at varying ambient conditions.

Strategies involving data analytics have also been used in the past; these have relied on conventional machine learning techniques such as Support Vector Machines (SVM) [16]–[18] and Neural Networks [19], [20]. In [17], [18], the authors used a SVM, however constant pulse discharge/charge profiles were mostly used in these works therefore the model's ability to generalize to dynamic real world scenarios is unknown.

Since Kalman Filters (KF) are extensively used for state estimation of systems, they have also been implemented in conjunction with classical machine learning methods to estimate SOC. In specific, these studies have used traditional machine learning techniques like ANN [21], Extreme Learning Machines [22], and Support Vector Machines [23], [24]. In [21], an ANN estimates the terminal voltage which is then fed into an Adaptive Extended Kalman Filter (EKF) that estimates SOC with a Root Mean Square (RMS) error of 2%. In [22], a single ambient temperature of 25 °C is considered and the estimation error is claimed to be below 1.5%. However, the extreme learning machine is trained on

Manuscript received March 31, 2017; revised October 24, 2017 and accepted December 5, 2017.

Ephrem Chemali, Phillip J Kollmeyer, Ryan Ahmed and Ali Emadi are with the McMaster Institute for Automotive Research and Technology (MacAUTO), Department of Electrical and Computer Engineering, McMaster University, Hamilton, Ontario L8S 4K1, Canada (email: chemale@mcmaster.ca; kollmeyp@mcmaster.ca, mohamerm@mcmaster.ca, emadi@mcmaster.ca)

Matthias Preindl is with Department of Electrical Engineering, Columbia University in the City of New York, New York, NY 10027, USA (email: matthias.preindl@columbia.edu)

constant pulse discharging currents hence their performance in dynamic loading profiles, experienced in real world scenarios, is unknown. In [23], a SVM is used with a moving window to reduce the computational burden when modeling the battery and an adaptive EKF is used to estimate SOC. This work achieves a Mean Absolute Error (MAE) of less than 2%.

It is difficult not to notice the great strides achieved recently in the field of machine learning. Nowadays, machine learning algorithms have become deeply entrenched in our lives. They are used for content filtering in search engines, sentiment analysis on social media as well as natural language processing on smartphone devices, to name a few [25]. Recently, advancements in many of the above mentioned applications can be attributed to a subset of artificial neural networks referred to as Recurrent Neural Networks (RNN) [26] with Long Short-Term Memory (LSTM) cells [27].

In this paper, we showcase how recurrent neural networks with an LSTM cell, a machine learning technique, can accurately estimate SOC and can do so by self-learning the network parameters. Specifically, the unique contributions brought about in this work are the following: (1)The LSTM-RNN can map battery measurement signals like voltage, current and temperature directly to the battery state of charge, avoiding computationally intensive filters and inference algorithms like Kalman filters used in traditional SOC estimators. (2)The LSTM-RNN can learn its own parameters by using back-propagation algorithms like stochastic gradient descent when exposed to training data which can be composed of as little as a couple of drive cycles. This bears a stark difference to the strategies traditionally employed like lumped parameter models, equivalent circuit or electrochemical models which require a great deal of time and data to hand-engineer and parameterize. (3)One LSTM-RNN network can learn to estimate SOC throughout various different ambient temperature conditions which is beneficial since incumbent estimation techniques must use different models or different look-up tables for different ambient temperatures.

After a brief introduction, the second section will discuss the theory behind recurrent neural networks and Long Short-Term Memory cells. The third section will discuss the experimental battery cell test bench used for data acquisition. In the forth section, the performance of the LSTM-RNN is validated on a slew of tests with data recorded at constant as well as at varying ambient temperatures.

II. Recurrent Neural Networks for SOC Estimation

Since 2012, great advancements have been achieved in the field of speech recognition [28]–[30]. More recently, a team at Baidu Research has developed a deep learning speech recognition system called Deep Speech 2 which exceeds human-level accuracy [31]. The latter deep neural network was composed of many layers which included layers of RNNs. Recurrent neural networks are a class of ANN geared towards pattern recognition in sequential datasets. Some popular examples of this are speech recognition, natural language understanding and machine translation where characters or words are fed into the network sequentially. Aside from the latter applications, RNNs can be useful for just about any type of time series data [26]. However, classical RNNs are known to have issues with long-range dependencies where the gradient either explodes or vanishes during back-propagation [32], [33]. RNNs with Long Short-Term Memory (LSTM) cells [27] have had better success at capturing long-term dependencies within a sequence and are thus much more widely used for these types of applications.

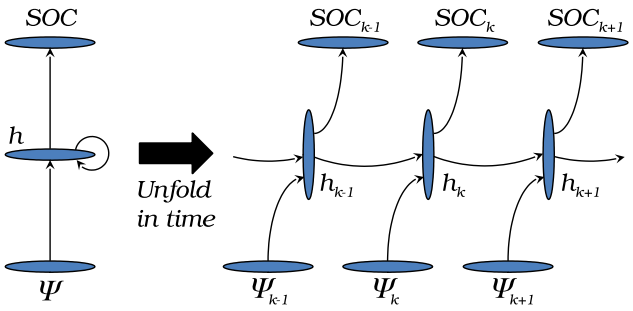

Fig. 1. Architecture of Recurrent Neural Network (left) and architecture of RNN unfolded in time (right). The input data is given by $\Psi_k = [V(k), I(k), T(k)]$ where $V(k), I(k)$ and $T(k)$ represent the voltage, current and temperature of the battery at time step k. h_{k-1} denotes the hidden layer of the LSTM-RNN at time step $k-1$. The output of the LSTM-RNN is the estimated SOC at every time step.

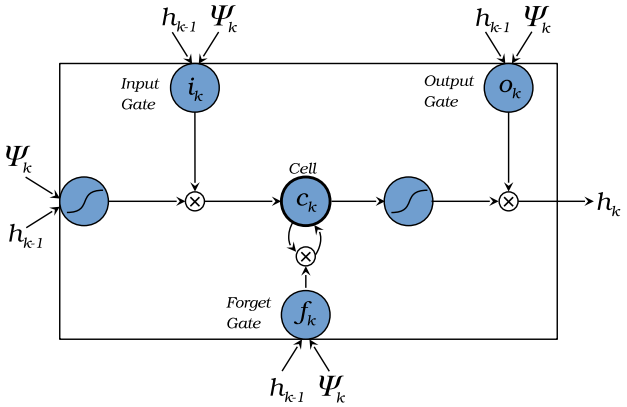

Fig. 2. Long Short-Term Memory cell. Ψ_k and h_{k-1} are the input data layer at current time step, k, and hidden layer at previous time step, $k-1$, respectively. i_k, o_k, f_k and c_k are the input, output and forget gates as well as the memory cell, respectively. Squiggly lines represent nonlinearities outlined in equation 1.

A LSTM-RNN, whose architecture is shown in figure 1, can represent nonlinear dynamic systems by mapping input sequences to output sequences. When we applied LSTM-RNNs towards SOC estimation, a typical dataset used to train the networks is given by $D = \{(\Psi_1, SOC_1^*), (\Psi_2, SOC_2^*), ..., (\Psi_N, SOC_N^*)\}$, where SOC_k^* is the ground-truth value or the observable state-of-charge value at time step k and Ψ_k is the vector of inputs also at time step k. The vector of inputs is defined as $\Psi_k =$

$[V(k), I(k), T(k)]$, where $V(k)$, $I(k)$, $T(k)$ are the voltage, current and temperature of the battery measured at time step k, respectively. The Long Short-Term Memory cell whose schematic representation is shown in figure 2, is equipped with a memory cell, c_k, which stores the long-term dependencies. During training, the input, output and forget gates allow the LSTM to forget or write new information to the memory cell. In this paper, TensorFlow [34], a machine learning framework, is used in conjunction with two Graphical Processing Units (GPU); the NVIDIA Titan X Pascal and a GeFORCE GTX 1080 TI. This framework provides the ability to quickly prototype and test different network architectures as a result of its ability to automatically compute backpropagation. The constructed networks incorporated TensorFlow's basic LSTM cell which is based on the LSTM unit discussed in [35] and can be represented by the following composite function,

$$\begin{aligned} i_k &= \eta(W_{\Psi i}\Psi_k + W_{hi}h_{k-1} + b_i) \\ f_k &= \eta(W_{\Psi f}\Psi_k + W_{hf}h_{k-1} + b_f) \\ c_k &= f_k c_{k-1} + i_k tanh(W_{\Psi c}\Psi_k + W_{hc}h_{k-1} + b_c) \\ o_k &= \eta(W_{\Psi o}\Psi_k + W_{ho}h_{k-1} + b_o) \\ h_k &= o_k tanh(c_k), \end{aligned} \tag{1}$$

where the initial hidden state, h_0, is set to a zero matrix, η is the sigmoid function and i, f, o and c are the input, forget, output gates and memory cell, respectively. They are called gates since they are a sigmoid function which can be zero valued thus possessing the ability to inhibit the flow of information to the next computational node. Each gate possesses its set of network weights which are denoted by W. The subscripts of W describe the transformation occuring between the two respective components, e.g. the input-output gate matrix is denoted by $W_{\Psi o}$, the hidden-input gate matrix is denoted by W_{hi}, etc. A bias, b, is added to the matrix multiplication at each gate to increase the networks flexibility to fit the data. A final fully-connected layer performs a linear transformation on the hidden state tensor h_k to obtain a single estimated SOC value at time step k. This is done as follows:

$$SOC_k = V_{out}h_k + b_y, \tag{2}$$

where V_{out} and b_y are the fully-connected layer's weight matrix and biases, respectively. The disparity between the LSTM-RNN's estimated SOC and the measured one is best represented by the following loss function computed at the end of each forward pass;

$$L = \sum_{k=0}^{N} \frac{1}{2}(SOC_k - SOC_k^*)^2, \tag{3}$$

where N is the length of the sequence and SOC_k as well as SOC_k^* are the estimated and ground truth values of SOC at time step k, respectively. A forward pass starts when the training data is fed into the network and ends when the SOC estimates are generated at each time step as well as when the errors and the overall loss are calculated. However, a training epoch, ϵ, includes one forward pass and one backward pass which is when the network weights, W, and biases, b, are updated. To do this, we used an optimization method called $Adam$ [36] to update the network weights and biases based on the gradient of the loss function. This is given by:

$$\begin{aligned} m_\epsilon &= \beta_1 m_{\epsilon-1} \nabla L(W_{\epsilon-1}) \\ r_\epsilon &= \beta_2 r_{\epsilon-1} \nabla L(W_{\epsilon-1})^2 \\ \widetilde{m}_\epsilon &= m_\epsilon / (1 - {\beta_1}^\epsilon) \\ \widetilde{r}_\epsilon &= r_\epsilon / (1 - {\beta_2}^\epsilon) \\ W_\epsilon &= W_{\epsilon-1} - \alpha \frac{\widetilde{m}_\epsilon}{\widetilde{r}_\epsilon - \kappa}, \end{aligned} \tag{4}$$

where, L is the loss function, β_1 and β_2 are decay rates set to 0.9 and 0.999, respectively, $\alpha = 10^{-4}$ is the training step size and κ is a constant term set to 10^{-8}. W_ϵ denotes the matrix of network parameters at the current training epoch and can be a placeholder for $W_{\Psi i}$, W_{hi}, $W_{\Psi f}$, etc. These gate matrices, the output weight matrix, V_{out}, as well as the biases are initialized with a normally distributed random number generator having mean 0 and standard deviation of 0.05. It is only during training that a forward and backward pass are performed to continuously update the network weights until a convergence criteria is met. With the backward pass, the network self-learns its weights, offering significant improvements over traditional SOC estimation strategies which require the time-consuming construction and parameterization of hand-engineered battery models.

During validation, a forward pass is solely required to generate the estimated SOC values at each time step and no backward pass is needed since the network parameters have already been learned during training. The LSTM-RNN offers an advantage of lower computational overhead, once trained, since a forward pass is comprised of a series of matrix multiplications. This, in general, is less computationally intensive than other algorithms, which might contain differential equations, for example. In addition, the LSTM-RNN, as will be shown in the results section of this paper, has the ability to encode the characteristic behavior of a battery at numerous ambient temperatures thus reducing the memory required to store different parameters for different ambient temperatures as is typically done for traditional battery models. Therefore, these latter advantages make LSTM-RNN a great candidate to perform estimation on many cells in a battery pack.

Many unique drive cycles are concatenated to form the training dataset and when compiled, this typically has a length of over 100,000 time steps. It is not possible to enter a sequence as long as this into our GPU memory during training. Therefore, the LSTM-RNN models are trained by feeding one batch of the sequence at a time which is commonly performed while training LSTM-RNNs. This is referred to as unrolling the LSTM cell in time for $\widetilde{N}$ steps where $\widetilde{N}$ is the batch length holding a smaller value than the total training sequence length, N, such that $\widetilde{N} < N$. Usually, if the time constant of the inherent dynamics within the sequence is shorter than $\widetilde{N}$, then the LSTM-RNN can still capture the time dependencies.

To evaluate the estimation performance of our networks, a few different error functions are used. These include the Mean Absolute Error (MAE), the RMS error, the standard deviation of the errors (STDDEV) and the maximum error (MAX).

TABLE I
PANASONIC 18650PF CELL PARAMETERS

Nominal Open Circuit Voltage	3.6V
Capacity	Min. 2.75 Ah / Typ. 2.9 Ah
Min / Max Voltage	2.5V / 4.2V
Mass / Energy Storage	48g / 9.9Wh
Minimum Charging Temperature	10 °C
Cycles to 80% Capacity	500 (100% DOD, 25 °C)

TABLE II
TEST EQUIPMENT SPECIFICATIONS

Cycler Manufacturer	Digatron Firing Circuits
Test Channel Used	25A, 0-18V channel
Voltage / Current Accuracy	+/- 0.1% Full Scale
Data Acquisition Rate Used	10Hz
Thermal Chamber	Cincinatti Sub Zero ZP-8
Size	8 cu. Ft.
Accuracy	+/-0.5 °C

III. BATTERY SPECIFICATION, CYCLING EQUIPMENT, AND EXPERIMENTAL TESTS

A Panasonic 18650 battery cell with a lithium nickel cobalt aluminum oxide ($LiNiCoAlO_2$ or NCA) chemistry, similar to the cell used in some Tesla vehicles, was tested [37]. The battery, which is rated to have 43 mΩ dc resistance is described in Table I [37], [38]. All the testing was performed in a thermal chamber with cell testing equipment manufactured by Digatron Firing Circuits, as described in Table II and shown in figure 3a).

To generate training and validation data for the recurrent neural network, the battery was exposed to a selection of drive cycles at ambient temperatures ranging from 0 to 25°C. A set experimental procedure was used, as is described in figure 3b). A schematic of the experimental apparatus is shown in figure 3c). The thermal chamber was first set to 25°C followed by a 3 hour pause to allow the battery's internal temperature to reach 25°C. The battery was then fully charged with a constant current charge rate of 2.9 A (1C) followed by a constant voltage charge at 4.2 V which was terminated when current fell below 50 mA. The thermal chamber temperature was then set to the desired ambient temperature to record the subsequent drive cycle, and, in turn, this was paused for three hours again to allow the battery's internal temperature to reach steady state. The battery is then discharged using a drive cycle power profile which includes regenerative braking (i.e. charging) power if the ambient temperature is greater than or equal to 10°C, the minimum temperature for which the battery is rated to charge. The current sensor that is used to measure current and to calculate capacity has an error of less than 25mA. For the typical dataset, this sums to a cumulative error of under 40mAh which is small compared to the 2900mAh of battery capacity.

During experimentation, the battery was exposed to 10 drive cycles. Each dataset consisted of a random combination of different drive cycles which included HWFET, UDDS, LA92 and US06. Constructing these unique datasets which were composed of various drive cycles, having a spectrum of different dynamics, provided the LSTM-RNN with a broad

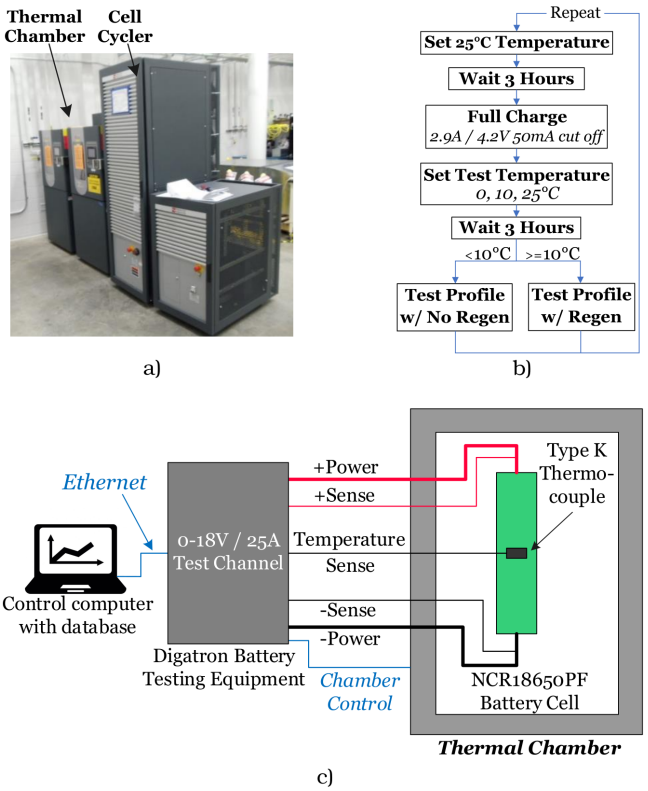

Fig. 3. a) Equipment used for battery testing, b) battery test procedure and c) schematic of the test bench and data logging system.

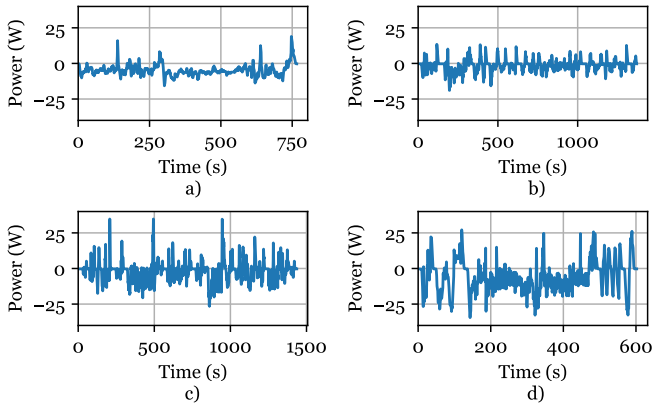

Fig. 4. Drive cycle power profiles, scaled for a single cell of 35kWh pack for a Ford F150 electric truck. a) HWFET, b) UDDS, c) LA92, d) US06.

range of realistic driving conditions. These 10 cycles were applied on the battery at three different ambient temperatures (0, 10, or 25 °C). Training of the LSTM-RNN is performed on a subset of these 10 cycles (typically 8 to 9 cycles) and will henceforth be referred to as the training data while validation is performed on a completely different subset of cycles (usually 1 or 2) which are henceforth referred to as test cases. An additional test case, called the Charging Test Case, is recorded at 25 °C to examine the network's performance over a charging profile. Furthermore, a second additional test case is recorded during experimentation which exposes the battery cell to an

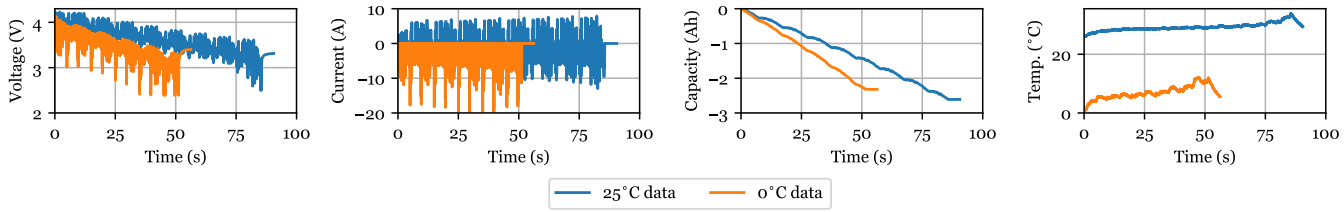

Fig. 5. US06 drive cycle recorded at an ambient temperature of 25 °C and 0 °C. The following measured quantities are shown from left to right; Voltage, Current, Amp-hours, battery surface temperature

ambient temperature increasing from 10 to 25 °C and is used to validate the LSTM-RNN's ability to adapt to a varying temperature. The drive cycle power profiles used are for an electric Ford F150 truck [39], [40], with the power profile scaled for a single cell of a 35 kWh pack consisting of 3,680 of the Panasonic NCR18650PF cells. The power profile for the drive cycles has discharge power (negative power) as great as 40 W per cell and charge power (positive power) as great as 35 W per cell, as is shown in figure 4. This translates to peak current of around 18 A, or 6C, which is a fairly typical peak C-rate for an electric vehicle application. The power profile is repeated until the battery's usable capacity is depleted. This is defined as 2.61 Ah when discharged at an ambient temperature of 25 °C, 2.5 Ah at 10 °C and 2.32 Ah at 0 °C.

The measured voltage, current, amp-hours, and battery surface temperature are shown in figure 5 for the US06 drive cycle at an ambient temperature of 25 °C and 0 °C. At 25 °C the current is relatively low, $\leq$3C, and the battery voltage drop is not too significant. The temperature, measured at the surface of the cylindrical cell with a thermocouple, increases by a few degrees over the first 70 minutes of the drive, and then spikes to 34 °C as the terminal voltage falls, resistance increases, and the loss therefore increases. At 0 °C, the battery resistance is much higher, resulting in significant voltage drop as is shown in figure 5. The higher resistance coupled with no regenerative braking energy due to the low temperature state, results in the drive cycle being repeated for 50 minutes at 0 °C, while this was repeated for 85 minutes at 25 °C. The battery also heats significantly, up to 13 °C, due to the higher loss at low temperature.

Although the LSTM-RNN showcased in this paper is trained on data obtained from a Panasonic 18650PF cell, the same LSTM-RNN can be trained on any other type of battery cell. The network architecture will not change from one battery cell to another. The network might need to be retrained for a completely different battery, but it's architecture and the values of the network hyperparameters, like the learning rate, will not change. This is not any different than traditional estimation techniques which must re-parameterize the battery models for different types of batteries.

IV. State of Charge Estimation Results

As mentioned above, the vector of inputs fed into the LSTM-RNN is defined as $\Psi_k = [V(k), I(k), T(k)]$, where $V(k)$, $I(k)$, $T(k)$ are the voltage, current and temperature measurements of the battery at time step k, respectively. The mixed drive cycles were logged at a sampling frequency of 1 Hz and they ranged roughly between 4000 and 10000 seconds long. The following two subsections investigate the LSTM-RNN's SOC estimation accuracy when trained on a dataset recorded at a constant ambient temperature and at variable ambient temperatures, respectively.

TABLE III
SOC ESTIMATION ACCURACY OF LSTM-RNN TRAINED ON FIXED AMBIENT TEMPERATURE DATA

Test Case	MAE(%)	RMS(%)	STDDEV(%)	MAX(%)
Test Case 1 at 10°C *	0.807	1.075	0.710	2.819
Test Case 2 at 10°C *	1.252	1.541	0.898	4.312
Charging Test Case at 25°C **	0.688	0.856	0.510	4.000

*Results obtained with network having a depth in time of $\widetilde{N}$=500
**Results obtained with network having a depth in time of $\widetilde{N}$=1000

A. SOC estimation at Fixed Ambient Temperature

In this section, the network is trained on up to 8 mixed drive cycles while validation is performed on 2 discharge test cases. In addition, a third test case, called the Charging Test Case, which includes a charging profile is used to validate the networks performance during charging scenarios. In addition, the regenerative braking which results in charging currents of over 8 A, as can be seen from figure 5, allows us to test the network's performance at higher momentary charge rates. Regenerative braking charging current is not included for validation test cases recorded at the lower temperatures since the battery is not rated to charge at temperatures below 10°C Celsius. In the Charging Test Case, charging is performed at 1C (2.9A). There was interest in examining an even faster charge rate, but the 1C rate is already twice the datasheet's recommended charge rate so rates that are any higher than this are considered excessive and potentially dangerous. The LSTM-RNN's hidden layer has 500 computational nodes. A smaller number of computational nodes are possible, however the network can converge to a solution much quicker with a larger number of nodes while using a GPU. The computational time needed to train this network is about 4 hours.

The MAE achieved on each of the first two test cases is 0.807% and 1.252%, respectively. The MAE, RMS, STDDEV and MAX performance metrics for these three test cases are outlined in Table III. The LSTM-RNN also showed good performance when tested on the Charging Test Case where the

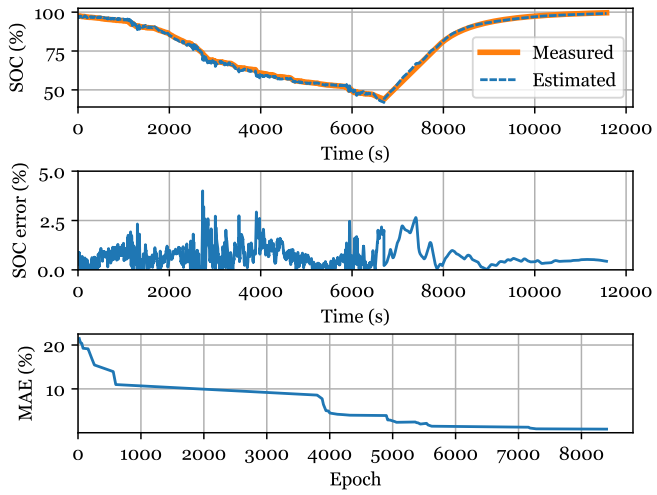

Fig. 6. LSTM-RNN tested on the Charging Test Case which includes discharge/charge profiles, recorded at ambient temperature of 25°C. LSTM-RNN architecture: network depth in time is $\widetilde{N}$ = 1000 and LSTM contains 500 nodes. MAE vs. the training epochs is also shown.

TABLE IV
SOC ESTIMATION ACCURACY OF LSTM-RNN WITH VARIOUS NETWORK DEPTHS IN TIME

Network Depth in Time ($\widetilde{N}$)	MAE(%)	RMS(%)	STDDEV(%)	MAX(%)
250	1.303	1.670	1.043	5.380
500	0.672	0.863	0.293	3.015
1000	0.573	0.690	0.148	2.569

Networks trained on data recorded at ambient temperature of 10°C

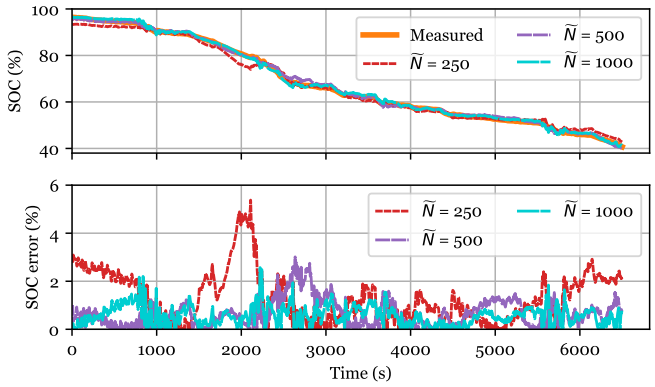

Fig. 7. Performance of 3 different LSTM-RNNs having depth in time of $\widetilde{N}$ = 250, 500, 1000, tested on Test Case 1 recorded at an ambient temperature of 10°C. Each of the three networks' LSTM cell contains 500 computational nodes. Table IV contains performance metric values.

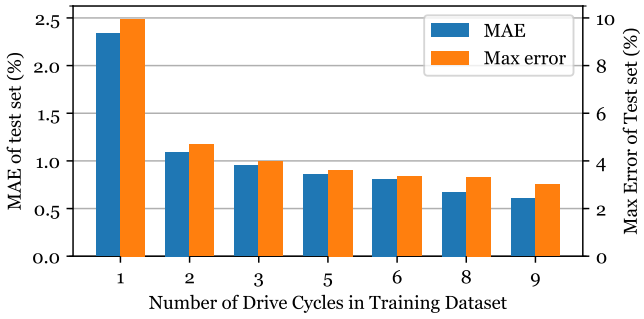

Fig. 8. LSTM-RNN trained on different amounts of training data at an ambient temperature of 10°C and tested on Test case 1. Training is stopped at 15000 epochs. LSTM-RNN architecture: network depth in time is $\widetilde{N}$ = 500 and LSTM contains 500 nodes.

MAE and MAX achieved is 0.688% and 4.000%, respectively. The estimation performance on the Charging Test Case is shown in figure 6. At the final training epoch, the error at every time step of the test case is shown in subplot 2. Also, at every training epoch, these errors over time are used to calculate the MAE. Therefore, a plot of MAE as a function of training epoch is shown in subplot 3.

We conduct various tests to understand the factors which influence the LSTM-RNN's estimation performance and to further validate this estimation strategy. In the first test, we trained three LSTM-RNNs having different depths in time, i.e. where $\widetilde{N}$ = 250, 500 and 1000 at an ambient temperature of 10°C. The estimated SOC and the error over time of these different LSTM-RNNs are shown in figure 7 and their performance metrics are outlined in Table IV. To maintain an unbiased comparison between the network architectures tested in Table IV training is stopped at 15000 epochs in each case. It is observed that the networks having larger depths in time which are exposed to more historical data perform better than those exposed to a smaller amount of historical data. However, the increase in estimation accuracy is not linearly proportional to depth in time since going from $\widetilde{N}$ = 250 to $\widetilde{N}$ = 500 reduces the MAE by about a half however, going from $\widetilde{N}$ = 500 to $\widetilde{N}$ = 1000 offers only a 15% reduction in MAE.

Another test is performed to measure the amount of training data needed to achieve good estimation accuracy. Therefore, instead of training the LSTM-RNN on a training dataset composed of 8 concatenated mixed drive cycles, as done to achieve the results in Table III, figure 6, figure 7 and Table IV, we record the estimation accuracy of LSTM-RNNs trained on different numbers of mixed drive cycles. This is shown in figure 8, where LSTM-RNNs are trained on one to nine mixed drive cycles and the MAE and max error measured over Test Case 1 are plotted in a bar graph. It is clear that the more training data the network is exposed to, the more accuracy is achieved, however after a certain amount of training data (6-8 drive cycles), we obtain diminishing returns. Interestingly, the LSTM-RNN is able to achieve a MAE of below 1% when training is conducted on 3 or more drive cycles. This can be very advantageous since the LSTM-RNN can learn it's network parameters and achieve accurate SOC estimates after being exposed to relatively small amounts of training data.

Two additional tests are conducted to examine the LSTM-RNN's performance when either an incorrect initialization is given to the network or when the test drive cycle begins at different SOC levels. Giving an LSTM-RNN an incorrect

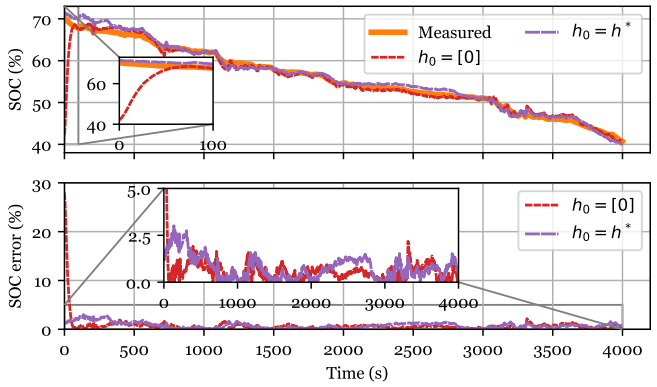

Fig. 9. Performance of LSTM-RNN with initial state of charge of 70%. Two different cases are tested; one with correct initialization of the hidden layer ($h_0 = h^*$) and the other with an incorrect initialization of the hidden layer ($h_0 = 0$). Please refer to text for further discussion.

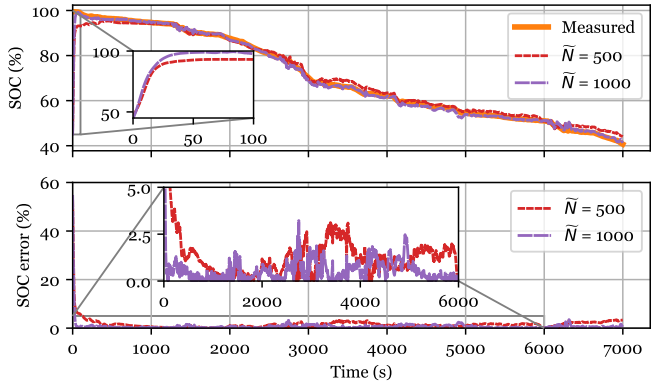

Fig. 10. Performance of LSTM-RNN given an incorrect initialization and starting at SOC of 100%. Two networks are tested; one having depth in time of $\widetilde{N}$ = 500 and the other having depth in time of $\widetilde{N}$ = 1000. LSTM contains 500 nodes in both networks.

initialization requires setting the hidden layer state at time step $k = 0$ to zero. This is the only way to test for the case of incorrect initialization since the input vector given to the LSTM-RNN at every time step includes $V(k)$, $I(k)$ as well as $T(k)$. SOC at time step $k-1$ or older are not used as feedback to the network. When correctly initialized, where $h_0 = h^*$, an LSTM-RNN achieves good performance with MAE = 0.776% on Test Case 1 which begins at SOC = 70%, shown in figure 9. When given an incorrect initialization, where $h_0 = 0$, the LSTM-RNN struggles to estimate SOC at the start of the drive cycle (SOC = 70%), where the error is about 27%, but quickly converges to a good state-of-charge estimate within the first 70 seconds of the drive cycle. Further validation is performed on this front by examining whether an LSTM-RNN that is deeper in time can converge quicker if given an incorrect initialization. This is shown in figure 10 where two LSTM-RNNs, one having depth in time of $\widetilde{N}$ = 500 and the other having $\widetilde{N}$ = 1000, are tested with incorrect initialization on Test Case 1 beginning at a SOC of 100%. It's clear that the LSTM-RNN which has a depth in time of $\widetilde{N}$ = 1000 seconds converges in less than 50 seconds which turns out to be faster than the LSTM-RNN having $\widetilde{N}$ = 500.

TABLE V
SOC ESTIMATION ACCURACY OF LSTM-RNN TRAINED ON MULTIPLE AMBIENT TEMPERATURE DATA

Ambient Temperature	MAE(%)	RMS(%)	STDDEV(%)	MAX(%)
25°C	0.774	1.110	0.796	3.692
10°C	0.782	0.995	0.616	4.047
0°C	2.088	2.444	1.270	6.687
Varying Temperature	1.606	2.038	1.256	5.815

B. SOC Estimation at Varying Ambient Temperatures

A LSTM-RNN is constructed to handle a larger training dataset which is composed of 27 drive cycles. These 27 drive cycles include three sets of 9 drive cycles; each set is recorded at 0°C, 10°C and 25°C. Another different mixed drive cycle, which is not a part of the training data, is used as a test case to validate the network's performance at each temperature. In particular, there are two goals that we desired to achieve within this second study. The first is to train the LSTM-RNN on datasets recorded at more than one ambient temperature such that one single LSTM-RNN can estimate SOC at different ambient temperature conditions. The second goal is to examine the LSTM-RNN's capability to interpolate its ability to estimate SOC at ambient temperatures different than the ones on which it was trained. The LSTM cell used in this study is unrolled for $\widetilde{N}$ = 1000 time steps and the time required to train this network is about 9 hours.

The estimation performance of this single LSTM-RNN is shown in figure 11 where estimation performed at 25°C, 10°C and 0°C are plotted in a), b) and c), respectively. The MAE achieved at these three ambient temperatures is 0.774, 0.782 and 2.088. The MAE, RMS, STDDEV and MAX metrics achieved over all three ambient temperatures are outlined in Table V. The performance is good and validates the LSTM-RNN's ability to encode the dynamics experienced by a Li-ion battery at various ambient temperatures into the parameters of a single network.

The single LSTM-RNN performed well for estimation on the validation test cases recorded at three different constant ambient temperatures however, battery-powered vehicles can undergo a change in ambient temperature of more than 10°C over the course of one day depending on the climate or the geographical location within which they operate. Hence, an interesting test is to examine its performance on a test case, not included in the training data, which is recorded at a changing ambient temperature. Therefore, the LSTM-RNN's performance over a test case where the ambient temperature in the thermal chamber is increased from 10°C to about 25°C is shown in Table V and in figure 12. The MAE achieved on this test case is 1.606% and showcases the LSTM-RNN's ability to perform estimation at ambient temperatures between 10°C and 25°C to which it is not exposed during the training process. This can be a great advantage if training data is scarce.

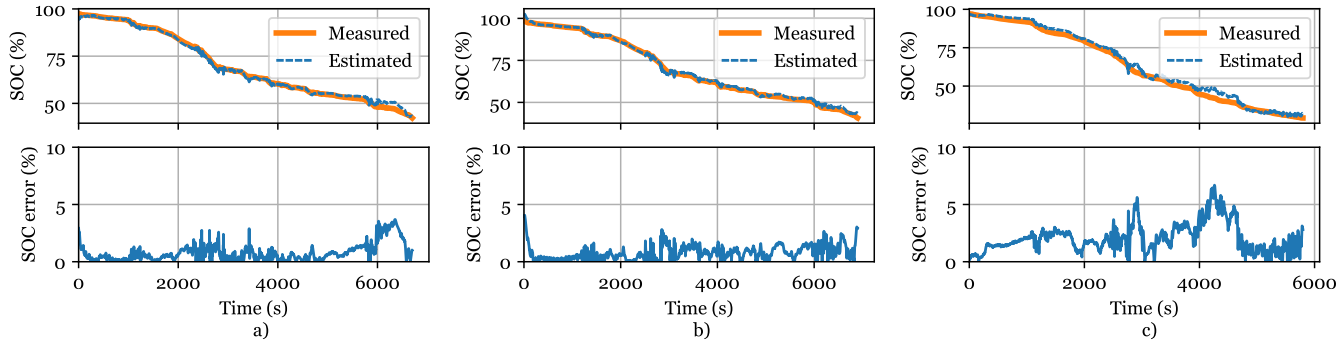

Fig. 11. Performance of a single LSTM-RNN on Test Case 1 performed at ambient temperatures of a) 25°C, b) 10°C and c) 0°C. LSTM-RNN architecture: network depth in time is $\widetilde{N}$ = 1000 and LSTM contains 500 nodes.

TABLE VI
COMPARISON OF SOC ESTIMATION ERROR FOR SIX STUDIES

Method	Error	Temperature	Test Case	Li-ion Battery
AEKF with ANN battery model [21]	<3% RMS	20°C (ambient)	+/-1A charging pulse profile	1.2Ah
AUKF w/ extreme learning machine battery model [22]	<1.5% MAX	25°C (ambient)	0.52A 50% duty cycle pulse discharge	2.6Ah Samsung
AUKF with LSSVM battery model [23]	<2% MAE	25°C to 42°C	Two drive cycles, +410 to -224A	70Ah Kokam
Fuzzy NN with genetic algorithm [19]	<0.9% APE	25°C (ambient)	Constant resistance discharge (13A)	10Ah MRL/ITRI
Radial Bias Function NN [20]	0.02% AAPE	Unspecified	Constant discharge rate (0.3C, 1C, 0.7C)	10Ah Lyno Power LYS347094S
LSTM-RNN (estimator in this paper)	0.6% MAE, 0.7% RMS, 2.6% MAX, (25°C)	0, 10, and 25°C (ambient)	Dynamic drive cycles, +/- 18A, Range of ambient temperatures	2.9Ah Panasonic NCR18650PF

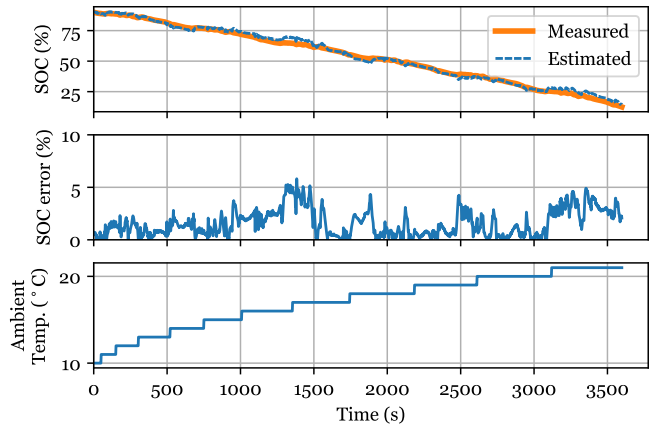

Fig. 12. LSTM-RNN validated over UDDS test case with rising ambient temperature. From the top; measured SOC compared to estimated SOC, the error and the ambient temperature vs. time. LSTM-RNN architecture: depth in time is $\widetilde{N}$ = 1000 and LSTM contains 500 nodes.

V. CONCLUSION

In the final analysis, this work offers three unique contributions. The contribution on the battery modeling front is how the LSTM-RNN maps battery measurements like voltage, current and temperature directly to SOC. The LSTM-RNN offers competitive estimation performance when compared to other algorithms mentioned in literature which are shown in Table VI. The contribution on the parameterization front is how the training algorithm self-learns all the network parameters; freeing researchers from hand-engineering and parameterizing the models themselves. In traditional methods, only after the parameters are fitted to a battery model, and after the time-consuming covariance matrix in a Kalman filter is determined, for example, can the algorithm operate in the field. In the third contribution, the elegance of this machine learning technique is that it allows us to encode the characteristic behavior at different ambient temperatures within the network while maintaining great estimation accuracy at these different ambient temperatures. In summary, the LSTM-RNN is exposed to extensive validation and achieves good performance. Consequently, this type of machine learning algorithm is proved to be a powerful tool for Li-ion battery SOC estimation and potentially other battery diagnostic strategies which are considered in future works. Given the amount of data generated by energy storage systems, it becomes natural to consider machine learning algorithms to perform state and parameter estimation and this work showcases how these algorithms can self-learn their own parameters, even when exposed to scarce datasets, and achieve competitive estimation performance.

VI. ACKNOWLEDGEMENTS

This research was undertaken, in part, through funding from the Canada Excellence Research Chair in Hybrid Powertrain Program. Battery testing is performed at the Wisconsin Energy Institute at the University of Wisconsin-Madison. We grate-

fully acknowledge the support of NVIDIA Corporation with the donation of the Titan X Pascal GPU used for this research.

REFERENCES

[1] "World Energy Outlook, Special Report Energy and Air Pollution," International Energy Agency, 2016.

[2] A. Emadi, *Advanced Electric Drive Vehicles*. New York: CRC Press, 2015.

[3] E. Chemali, M. Preindl, P. Malysz, and A. Emadi, "Electrochemical and electrostatic energy storage and management systems for electric drive vehicles: State-of-the-art review and future trends," *IEEE Journal of Emerging and Selected Topics in Power Electronics*, vol. 4, no. 3, pp. 1117–1134, 2016.

[4] P. Malysz, R. Gu, J. Ye, H. Yang, and A. Emadi, "State-of-charge and state-of-health estimation with state constraints and current sensor bias correction for electrified powertrain vehicle batteries," *IET Electrical Systems in Transportation*, p. 9 pp., 2016.

[5] L. McCurlie, M. Preindl, and A. Emadi, "Fast model predictive control for redistributive lithium-ion battery balancing," *IEEE Transactions on Industrial Electronics*, vol. 64, no. 2, pp. 1350–1357, 2017.

[6] W. Waag, C. Fleischer, and D. U. Sauer, "Critical review of the methods for monitoring of lithium-ion batteries in electric and hybrid vehicles," *Journal of Power Sources*, vol. 258, pp. 321 – 339, 2014.

[7] R. Ahmed, M. El Sayed, I. Arasaratnam, J. Tjong, and S. Habibi, "Reduced-Order Electrochemical Model Parameters Identification and SOC Estimation for Healthy and Aged Li-Ion Batteries. Part I: Parameterization Model Development for Healthy Batteryies," *IEEE Journal of Emerging and Selected Topics in Power Electronics*, vol. 2, no. 3, pp. 659–677, 2014.

[8] R. Ahmed, M. El Sayed, I. Arasaratnam, J. Tjong, and S. Habibi, "Reduced-Order Electrochemical Model Parameters Identification and State of Charge Estimation for Healthy and Aged Li-Ion Batteries - Part II: Aged Battery Model and State of Charge Estimation," *IEEE Journal of Emerging and Selected Topics in Power Electronics*, vol. 2, no. 3, pp. 678–690, 2014.

[9] M. A. Roscher and D. U. Sauer, "Dynamic electric behavior and open-circuit-voltage modeling of LiFePO4-based lithium ion secondary batteries," *Journal of Power Sources*, vol. 196, no. 1, pp. 331 – 336, 2011.

[10] J. Li, J. K. Barillas, C. Guenther, and M. A. Danzer, "A comparative study of state of charge estimation algorithms for lifepo4 batteries used in electric vehicles," *Journal of Power Sources*, vol. 230, pp. 244 – 250, 2013.

[11] L. Liu, L. Y. Wang, Z. Chen, C. Wang, F. Lin, and H. Wang, "Integrated system identification and state-of-charge estimation of battery systems," *IEEE Transactions on Energy Conversion*, vol. 28, no. 1, pp. 12–23, Mar. 2013.

[12] M. Gholizadeh and F. Salmasi, "Estimation of state of charge, unknown nonlinearities, and state of health of a lithium-ion battery based on a comprehensive unobservable model," *IEEE Transactions on Industrial Electronics*, vol. 61, no. 3, pp. 1335–1344, Mar. 2014.

[13] X. Chen, W. Shen, Z. Cao, and A. Kapoor, "A novel approach for state of charge estimation based on adaptive switching gain sliding mode observer in electric vehicles," *Journal of Power Sources*, vol. 246, pp. 667 – 678, 2014.

[14] C. Hu, B. D. Youn, and J. Chung, "A multiscale framework with extended kalman filter for lithium-ion battery {SOC} and capacity estimation," *Applied Energy*, vol. 92, pp. 694 – 704, 2012.

[15] F. Sun, X. Hu, Y. Zou, and S. Li, "Adaptive unscented kalman filtering for state of charge estimation of a lithium-ion battery for electric vehicles," *Energy*, vol. 36, no. 5, pp. 3531 – 3540, 2011.

[16] T. Hansen and C.-J. Wang, "Support vector based battery state of charge estimator," *Journal of Power Sources*, vol. 141, no. 2, pp. 351 – 358, 2005.

[17] J. A. Anton, P. G. Nieto, F. de Cos Juez, F. S. Lasheras, M. G. Vega, and M. R. Gutierrez, "Battery state-of-charge estimator using the {SVM} technique," *Applied Mathematical Modelling*, vol. 37, no. 9, pp. 6244 – 6253, 2013.

[18] J. C. A. Anton, P. J. G. Nieto, C. B. Viejo, and J. A. V. Vilan, "Support vector machines used to estimate the battery state of charge," *IEEE Transactions on Power Electronics*, vol. 28, no. 12, pp. 5919–5926, 2013.

[19] Y. S. Lee, W. Y. Wang, and T. Y. Kuo, "Soft computing for battery state-of-charge (bsoc) estimation in battery string systems," *IEEE Transactions on Industrial Electronics*, vol. 55, no. 1, pp. 229–239, 2008.

[20] W.-Y. Chang, "Estimation of the state of charge for a lfp battery using a hybrid method that combines a rbf neural network, an ols algorithm and aga," *International Journal of Electrical Power & Energy Systems*, vol. 53, pp. 603–611, 2013.

[21] M. Charkhgard and M. Farrokhi, "State-of-charge estimation for lithium-ion batteries using neural networks and ekf," *IEEE transactions on industrial electronics*, vol. 57, no. 12, pp. 4178–4187, 2010.

[22] J. Du, Z. Liu, and Y. Wang, "State of charge estimation for li-ion battery based on model from extreme learning machine," *Control Engineering Practice*, vol. 26, pp. 11–19, 2014.

[23] J. Meng, G. Luo, and F. Gao, "Lithium polymer battery state-of-charge estimation based on adaptive unscented kalman filter and support vector machine," *IEEE Transactions on Power Electronics*, vol. 31, no. 3, pp. 2226–2238, 2016.

[24] Z. Deng, L. Yang, Y. Cai, H. Deng, and L. Sun, "Online available capacity prediction and state of charge estimation based on advanced data-driven algorithms for lithium iron phosphate battery," *Energy*, vol. 112, pp. 469–480, 2016.

[25] Y. LeCun, Y. Bengio, and G. Hinton, "Deep learning," *Nature*, vol. 521, no. 7553, pp. 436–444, 2015.

[26] I. Sutskever, "Training Recurrent neural Networks," Ph.D. dissertation, University of Toronto, 2013.

[27] S. Hochreiter and J. Schmidhuber, "Long short-term memory," *Neural Computation*, vol. 9, no. 8, pp. 1735–1780, 1997.

[28] G. Hinton, L. Deng, D. Yu, G. E. Dahl, A. r. Mohamed, N. Jaitly, A. Senior, V. Vanhoucke, P. Nguyen, T. N. Sainath, and B. Kingsbury, "Deep neural networks for acoustic modeling in speech recognition: The shared views of four research groups," *IEEE Signal Processing Magazine*, vol. 29, no. 6, pp. 82–97, Nov. 2012.

[29] G. E. Dahl, D. Yu, L. Deng, and A. Acero, "Context-dependent pre-trained deep neural networks for large-vocabulary speech recognition," *IEEE Transactions on Audio, Speech, and Language Processing*, vol. 20, no. 1, pp. 30–42, 2012.

[30] A. Graves, A.-r. Mohamed, and G. Hinton, "Speech Recognition with Deep Recurrent Neural Networks," *2013 IEEE International Conference on Acoustics, Speech and Signal Processing (ICASSP)*, no. 3, pp. 6645–6649, 2013.

[31] D. Amodei, R. Anubhai, E. Battenberg, C. Case, J. Casper, B. Catanzaro, J. Chen, M. Chrzanowski, A. Coates, G. Diamos, E. Elsen, J. Engel, L. Fan, C. Fougner, T. Han, A. Hannun, B. Jun, P. LeGresley, L. Lin, S. Narang, A. Ng, S. Ozair, R. Prenger, J. Raiman, S. Satheesh, D. Seetapun, S. Sengupta, Y. Wang, Z. Wang, C. Wang, B. Xiao, D. Yogatama, J. Zhan, and Z. Zhu, "Deep Speech 2: End-to-End Speech Recognition in English and Mandarin," *ArXiv e-prints*, Dec. 2015.

[32] R. Pascanu, T. Mikolov, and Y. Bengio, "On the difficulty of training recurrent neural networks." *30th International Conference on Machine Learning (ICML)*, vol. 28, pp. 1310–1318, 2013.

[33] S. Hochreiter, "The vanishing gradient problem during learning recurrent neural nets and problem solutions," *International Journal of Uncertainty, Fuzziness and Knowledge-Based Systems*, vol. 06, no. 02, pp. 107–116, 1998.

[34] M. Abadi, A. Agarwal, P. Barham, E. Brevdo, Z. Chen, C. Citro, G. S. Corrado, A. Davis, J. Dean, M. Devin, S. Ghemawat, I. Goodfellow, A. Harp, G. Irving, M. Isard, Y. Jia, R. Jozefowicz, L. Kaiser, M. Kudlur, J. Levenberg, D. Mané, R. Monga, S. Moore, D. Murray, C. Olah, M. Schuster, J. Shlens, B. Steiner, I. Sutskever, K. Talwar, P. Tucker, V. Vanhoucke, V. Vasudevan, F. Viégas, O. Vinyals, P. Warden, M. Wattenberg, M. Wicke, Y. Yu, and X. Zheng, "TensorFlow: Large-scale machine learning on heterogeneous systems," 2015, software available from tensorflow.org. [Online]. Available: http://tensorflow.org/

[35] W. Zaremba, I. Sutskever, and O. Vinyals, "Recurrent neural network regularization," *arXiv preprint arXiv:1409.2329*, 2014.

[36] D. P. Kingma and J. Ba, "Adam: A method for stochastic optimization," *CoRR*, vol. abs/1412.6980, 2014.

[37] Panasonic, "Panasonic NCR18650PF Lithium-Ion Battery Datasheet (June 2016)," 2016.

[38] Panasonic, "Introduction of NCR18650PF, Panasonic," 2013.

[39] P. J. Kollmeyer, "Development and Implementation of a Battery-Electric Light-Duty Class 2a Truck including Hybrid Energy Storage," Ph.D. dissertation, The University of Wisconsin - Madison, 2015.

[40] P. J. Kollmeyer, W. Lamb, L. W. Juang, J. D. McFarland, T. M. Jahns, and B. Sarlioglu, "Design of an electric powertrain for a ford f150 crew cab truck utilizing a lithium battery pack and an interior pm synchronous machine drive," in *2012 IEEE Transportation Electrification Conference and Expo (ITEC)*, pp. 1–8, 2012.

Ephrem Chemali received the Honours B.Sc. degree in Physics and the M.Sc. in Atomic Physics degree from York University, Toronto, in 2009 and in 2011, respectively. After completing his M.Sc., he worked as an engineering lead and project manager for Moose Power, a photovoltaic solar rooftop developer, where he managed the interconnection of 1.7 MW of rooftop solar projects.

Ephrem is currently a Ph.D. Candidate at the McMaster Institute for Automotive Research and Technology (MacAUTO) where his research work includes applying machine learning techniques to Energy Management Systems as well as building next generation power electronic converters for electric drive vehicles. In 2014, he served as the Energy Storage System team lead and Project Manager for the McMaster Engineering EcoCAR 3 team. Their work on a Hybrid Energy Storage System designed for a Plug-in Hybrid Electric 2016 Chevrolet Camaro earned them a 2nd place finish in the innovation category of the EcoCAR 3 Year 1 Competition (2015). His research interests lie in next generation Energy Storage Systems and Artificial Intelligence.

Phillip J Kollmeyer Phillip Kollmeyer (IEEE S04-M16) received the B.S.(2006), M.S.(2011), and Ph.D.(2015) degrees in electrical engineering from the University of Wisconsin-Madison, USA with a focus in the area of electric drivetrain design and energy storage. As a graduate student, he built a heavily instrumented prototype light-duty electric truck and led the development of a new energy storage test facility. He also performed a range of projects on hybrid energy storage, battery aging, and battery and ultracapacitor modeling, and received two awards for his teaching in the electric machines and drives area. Since 2016 he has worked on a variety of independent consulting projects. He is currently a Post-Doctoral fellow at McMaster University, Hamilton, ON, Canada, where his focus is energy storage research for transportation applications.

Matthias Preindl is an Assistant Professor in the Department of Electrical Engineering, Columbia University in the City of New York, USA. He received the PhD degree in Energy Engineering from the Doctoral School of Industrial Engineering at University of Padua, Italy (2014), the MSc degree in Electrical Engineering and Information Technology from ETH Zurich, Switzerland (2010), and the BSc degree in Electrical Engineering (summa cum laude) form University of Padua, Italy (2008).

M. Preindl was a Sessional Professor in the Department of Electrical and Computer Engineering (2015) and a Post Doctoral Research Associate at the McMaster Institute for Automotive Research and Technology (2014-2015), both at McMaster University, Canada. He was a visiting scholar at University of California, Berkeley, USA (2013), a visiting student at Aalborg University, Denmark (2009), and a trainee at the National Research Council (CNR), Italy (2008). M. Preindl actively collaborates with industry partners on a project basis and he was with Leitwind AG, Italy, where he worked as an R&D engineer in Power Electronic and Drives (2010-2012).

M. Preindl obtained several honors including merit-based fellow and scholarships, a price for outstanding achievements during his studies, and best presentation awards. His primary research interests are the design and control of power electronic and motor drive systems with applications in electrified transportation systems, renewable-energy power plants, and smart grids.

Ryan Ahmed Ryan Ahmed is currently an adjunct assistant professor at the Department of Mechanical Engineering at McMaster University in Ontario, Canada. Dr. Ryan holds a doctorate degree in Mechanical Engineering, with focus on Mechatronics and Battery Management Systems from McMaster University. He received a Masters degree in Mechanical Engineering from McMaster, with specialization in Artificial Intelligence (AI) and engine fault detection. Dr. Ryan has taught several courses on management and control of electric vehicles at McMaster University and at the educational EV/HEV boot camp at the IEEE Transportation Electrification Conference and Expo (ITEC 2015) in MI, USA. He is a Stanford Certified Project Manager (SCPM), certified Professional Engineer (P.Eng.) in Ontario, a member of the Society of Automotive Engineers (SAE), and a member of the Institute of Electrical and Electronics Engineers (IEEE). He was a recipient of the Best Paper Award at the IEEE Transportation Electrification Conference and Expo, Dearborn, MI, USA, in 2012.

Ali Emadi (IEEE S98-M00-SM03-F13) received the B.S. and M.S. degrees in electrical engineering with highest distinction from Sharif University of Technology, Tehran, Iran, in 1995 and 1997, respectively, and the Ph.D. degree in electrical engineering from Texas A&M University, College Station, TX, USA, in 2000. He is the Canada Excellence Research Chair in Hybrid Powertrain at McMaster University in Hamilton, Ontario, Canada. Before joining McMaster University, Dr. Emadi was the Harris Perlstein Endowed Chair Professor of Engineering and Director of the Electric Power and Power Electronics Center and Grainger Laboratories at Illinois Institute of Technology (IIT) in Chicago, Illinois, USA, where he established research and teaching facilities as well as courses in power electronics, motor drives, and vehicular power systems. He was the Founder, Chairman, and President of Hybrid Electric Vehicle Technologies, Inc. (HEVT) - a university spin-off company of IIT. Dr. Emadi has been the recipient of numerous awards and recognitions. He was the advisor for the Formula Hybrid Teams at IIT and McMaster University, which won the GM Best Engineered Hybrid System Award at the 2010, 2013, and 2015 competitions. He is the principal author/coauthor of over 350 journal and conference papers as well as several books including Vehicular Electric Power Systems (2003), Energy Efficient Electric Motors (2004), Uninterruptible Power Supplies and Active Filters (2004), Modern Electric, Hybrid Electric, and Fuel Cell Vehicles (2nd ed, 2009), and Integrated Power Electronic Converters and Digital Control (2009). He is also the editor of the Handbook of Automotive Power Electronics and Motor Drives (2005) and Advanced Electric Drive Vehicles (2014). Dr. Emadi was the Inaugural General Chair of the 2012 IEEE Transportation Electrification Conference and Expo (ITEC) and has chaired several IEEE and SAE conferences in the areas of vehicle power and propulsion. He is the founding Editor-in-Chief of the IEEE Transactions on Transportation Electrification.